



RESEARCH LETTER

10.1002/2014GL061863

Key Points:

- We present detailed observations of a field-scale turbidity current
- We demonstrate the existence of multiple flow phases within the same flow event
- The dynamics of the turbidity current head differed from current paradigms

Supporting Information:

- Readme

Correspondence to:

E. J. Sumner,
esther@mbari.org

Citation:

Sumner, E. J., and C. K. Paull (2014), Swept away by a turbidity current in Mendocino submarine canyon, California, *Geophys. Res. Lett.*, *41*, 7611–7618, doi:10.1002/2014GL061863.

Received 17 SEP 2014

Accepted 17 OCT 2014

Accepted article online 21 OCT 2014

Published online 11 NOV 2014

Swept away by a turbidity current in Mendocino submarine canyon, California

E. J. Sumner^{1,2} and C. K. Paull¹

¹Monterey Bay Aquarium Research Institute, Moss Landing, California, USA, ²Ocean and Earth Science, University of Southampton, Southampton, UK

Abstract We present unique observations and measurements of a dilute turbidity current made with a remotely operated vehicle in 400 m water depth near the head of Mendocino Canyon, California. The flow had a two-layer structure with a thin (0.5 to 30 m), relatively dense (<0.04 vol %) and fast (up to ~1.7 m/s) wedge-shaped lower layer overlain by a thicker (up to 89 m) more dilute and slower current. The fast moving lower layer lagged the slow moving, dilute flow front by 14 min, which we infer resulted from the interaction of two initial pulses. The two layers were strongly coupled, and the sharp interface between the layers was characterized by a wave-like instability. This is the first field-scale data from a turbidity current to show (i) the complex dynamics of the head of a turbidity current and (ii) the presence of multiple layers within the same event.

1. Introduction

Turbidity currents are sediment-laden flows that travel downslope, under the action of gravity, because they are denser than the surrounding ambient fluid. There are few direct measurements of turbidity currents when compared to other major sediment transport processes [Talling *et al.*, 2013; Puig *et al.*, 2014]; this is largely because of difficulties in predicting when a turbidity current will occur and a lack of techniques that can withstand and measure these flows. As a result, long term deployments of monitoring equipment are required in order to capture an event [Xu, 2011; Xu *et al.*, 2014]. Thus, the resolution of instrumentally recorded flow measurements is constrained by limitations of battery power and storage. For example, measurements are commonly collected on an hourly basis, and even then, they must be averaged over many minutes [e.g., Xu, 2010; Xu *et al.*, 2014; Cooper *et al.*, 2013]. Furthermore, due to signal attenuation and absorption, existing acoustic technologies for measuring flow velocity can only penetrate dilute flows and as a result of sidelobe reflections from the seafloor are incapable of measuring within ~6% of their height above the seabed [RDI Instruments, 2014]. Concentration measurements in ocean turbidity currents comprise (i) point measurements from transmissometers calibrated with grain-size samples [Xu, 2010; Xu *et al.*, 2014], (ii) profiles of acoustic backscatter that are a function of sediment concentration and grain size [Xu, 2010; Hughes Clarke *et al.*, 2014], and (iii) estimates of depth-averaged concentration calculated using flow parameters including flow depth, flow velocity, and seafloor gradient [Xu, 2010; Xu *et al.*, 2014]. Nevertheless, measurements of submarine turbidity currents are extraordinarily valuable in improving understanding of the nature of these enigmatic flows.

Fundamental questions remain about the nature of turbidity currents, including how well conceptual models, based on experimental analogues and inferences made from ancient deposits, represent the real world. Turbidity currents are often viewed as simple surges; however, the duration of flows, nature of triggering, and character of deposits all imply complexity in the evolution of turbidity currents [e.g., Piper *et al.*, 1999]. Here we present novel observations collected using a remotely operated vehicle (ROV) that got entrained in a turbidity current; they reveal the complex structure of the flow from the initial passage of the head through the main body. This data set provides direct evidence from a turbidity current that can be used to ground truth hypotheses of flow complexity that have previously been based on indirect evidence from experiments, numerical models, and ancient deposits.

2. Regional Setting

Mendocino Canyon is located offshore Cape Mendocino in Northern California (Figures 1a and 1b). The canyon head is located 4 km from the shoreline in an area characterized by a narrow (<15 km) continental

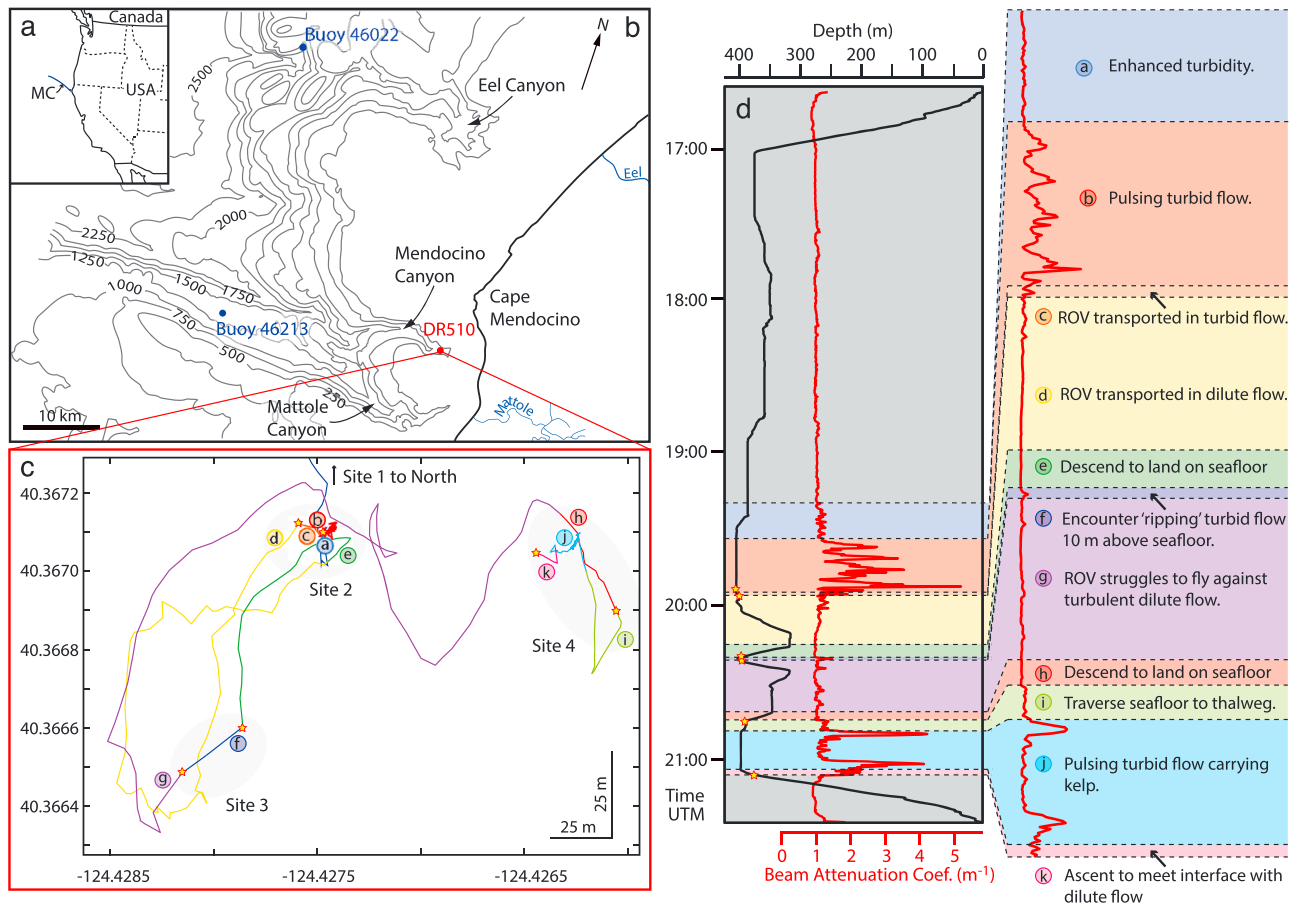


Figure 1. (a) Location of Mendocino Canyon (MC). (b) Location of the ROV dive sites and weather buoys. (c) Map showing the flight path of the ROV. (d) Timeline of events with the depth of the ROV and turbidity (BAC) shown. The colored letters refer to the key events shown in Figure 1d, and the yellow stars show points at which the thickness of the lower layer was measured.

shelf. Mendocino Canyon is bounded to the south by the Mendocino Escarpment, which is the surface expression of the triple junction separating the North American, Pacific, and Gorda tectonic plates.

Mendocino Canyon has received little scientific attention; indeed, no detailed bathymetric map could be found for the canyon head. Two piston cores and a box core have been collected in Mendocino Channel ~70 km downstream of the canyon head [Goldfinger et al., 2007]. These cores contained turbidity current deposits (turbidites) with an average recurrence interval of 34 years during the past 800 years. This suggests that Mendocino Canyon is the most active canyon on the Cascadia Margin, which extends from the Mendocino Escarpment 850 km north to Vancouver Island (Figure 1a). This high frequency of events is attributed to the location of the canyon, close to the triple junction, and the proximity of the canyon head to the shoreline, enabling capture of shelfal sediments [Goldfinger et al., 2007].

3. Methods

A dive (DR510) of the remotely operated vehicle (ROV) *Doc Ricketts* was conducted on 3 August 2013 in the head of Mendocino Canyon. The *Doc Ricketts* is operated from the ship R/V *Western Flyer*, which is a dynamically positioned (DP) vessel. The position of the ROV is continuously tracked using an ultrashort baseline system. The ROV was equipped with a high-definition camera that provides continuous video observations, a conductivity-temperature-depth (CTD) sensor (SBE 19plus), and a transmissometer (Wet Labs C-Star) located 1.25 m, 2.34 m, and 2.44 m above the base of the ROV, respectively. Depth adjustments were

made that accounted for the relative positions of different instruments. The video observations were recorded continuously, and the CTD and transmissometer data were recorded at 1 s intervals. The ROV was fitted with a vibracorer and could also take short push cores using its manipulator arm.

The transmissometer measures the transmission of light (A) through a fixed volume of water; these values were converted to a beam attenuation coefficient (BAC), using $BAC = -\frac{1}{z} \ln A$, where z is the transmissometer path length (0.25 m) [Sea-Bird Electronics, 2011]. BAC is linearly proportional to concentration for a wide range of grain sizes and types including clays [Guillén *et al.*, 2000; Xu *et al.*, 2014], and measurements of BAC from different depths were used to construct vertical profiles. BAC was not routinely converted to concentration because this requires knowledge of the grain-size distribution. In order to enable comparison with other studies, we calculated a range of potential concentrations for the maximum measured value of BAC using Xu *et al.*'s [2014] calibration curves and assuming a range of grain sizes.

4. Results

4.1. Observations During Doc Ricketts Dive 510

The original plan for 3 August was to dive on Eel Fan, 40 km to the northwest of Mendocino Canyon (Figure 1b); however, this plan was abandoned because wind and sea conditions precluded ROV operations at this site. National Buoy Data Center stations 46022 and 46213 (see Figure 1b for locations) show that winds were up to 11 m/s with wave heights of up to 2.6 m (20 min average of the highest one third of waves recorded) both from the north. These are not unusual wave conditions for this area; waves of this height and larger were experienced several times per month throughout 2013. Mendocino Canyon Head was chosen as an alternative dive site because it is in the lee of Cape Mendocino and proved adequately sheltered to conduct a dive. The plan was to collect a transect of vibracores across the axis of the canyon that would complement an existing data set for this margin. We did not have a detailed navigational chart to use during the dive; therefore, prior to launching the ROV, the R/V *Western Flyer* collected an echosounder profile along a transect across the dive site, thus enabling us to locate the thalweg. A series of annotated video clips can be found at <https://www.youtube.com/watch?v=43Hp2ETgIXM>.

The ROV landed on the seafloor in 372 m water depth on the canyon flank at site 1 (Figures 1c and 1d) at 17:01 universal time meridian (UTM). Visibility was excellent, and the pilots noted a gentle current flowing west down the canyon with water temperature of 6.31°C and salinity of 34.14 practical salinity unit (psu); based on our experience, gentle down-canyon currents are common during quiescent periods in submarine canyons. During the following 2.5 h, a series of push cores and vibracores were collected on a sampling transect moving toward the canyon thalweg. The thalweg was precisely located by flying the ROV along a cross-channel transect in order to locate the deepest point. At 19:20 UTM, the transmissometer first recorded an enhanced turbidity during a period that we were not coring and thus stirring up seafloor sediment (Figures 1c and 1d, event a). However, these turbidity levels were too subtle to be recognized in the video data, and there was no perceivable increase in the velocity or turbulence of the down-canyon current. The deepest point on the transect was reached at 19:30 UTM when the ROV landed on the seafloor in 405 m water depth facing up the canyon in order to take a series of cores directly from the canyon thalweg. At this time, visibility was still good, and the position of the R/V *Western Flyer* was fixed in DP. The down-canyon current was sufficient to transport particles over seafloor ripples (see annotated video - clip #2). At the onset of coring, the water temperature had increased to 6.94°C, and salinity had decreased to 34.07 psu despite an increase in water depth.

During 3 min (from 19:34 to 19:37 UTM), the video data show that the water gradually became more turbid until it was no longer possible to see the seafloor (Figures 1c and 1d, start of event b); these visual observations correlate with a gradual increase in BAC over the same time period. During the following 18 min (Figures 1c and 1d, event b), the ROV maintained its position on the seafloor, while pulses of more and less turbid water passed through the area with an average periodicity between complete "blackouts" of 5 min (based on the first four peaks in the transmissometer data: Figure 1d, event b). Visual observations show that the pulses correlate with changes in the thickness of the thin turbid near-bed flow. At its thinnest, the flow was seen to be billowing through the rack of push core tubes located on the front of the ROV; this constrains its thickness to ~0.5 m (see annotated video - clip #3). The top of this near-bed turbid flow was observed to be a sharp and billowing interface.

During the 18 min period that the ROV was on the bottom within the flowing turbid waters (Figures 1c and 1d, event b), the pilots noted that the lowermost section of the umbilical connecting the ROV to the ship was streaming out to the west, down canyon, even though the ship remained positioned to the east of the ROV. The pilots also noted that the current velocity was rapidly fluctuating about a mean down-canyon direction. Ultimately, the current spun the ROV around, and the pilots were forced to lift the vehicle off the seafloor in order to regain control of the vehicle. At the point that the ROV left the canyon floor, the water temperature had increased to 7.31°C, and salinity had decreased to 34.04 psu.

In the following 2 min, the ROV was transported ~14 m down canyon, despite efforts to fly at full speed in the opposite direction (Figures 1c and 1d, event c). The velocity of the ROV depends on its position relative to the ship and the length of the umbilical attaching it to the ship. The ROV was in a favorable position (flying toward the ship) to achieve its maximum velocity of 2 knots (~1 m/s), which has been measured on previous dives using a Doppler velocity log. In order to try to regain control, the ROV ascended 83 m to a water depth of 316 m. However, a strong turbulent current was experienced throughout this depth, and the ROV was swept 98 m farther down canyon before control was regained (Figures 1c and 1d, event d). While ascending, an abrupt billowing interface between the turbid and dilute flow was observed at a water depth of 402 m, which was 3 m above the thalweg. Thus, at this time, the flow comprised a thin turbid near-bed layer observed to increase from 0.5 to 3 m in thickness with a sharp billowing top overlain by a dilute ≥ 80 m thick turbulent layer.

Having regained control of the ROV after ascending to 316 m water depth, a return to the seafloor at site 2 was attempted. During the descent, the ROV was pushed 75 m southwest down the canyon (Figures 1c and 1d, event e). The descent was abandoned at 399 m water depth (Figures 1c and 1d, event f), which was 10 m above the seafloor according to the altimeter on the ROV (Figure 1c; site 3). At this depth, visibility was poor, and the current velocity made it unsafe to attempt to land the ROV on the seafloor; thus, the ROV again ascended to 316 m water depth in order to regain control.

The ROV proceeded to fly up canyon (with difficulty) at 347 m water depth (Figures 1c and 1d, event g), where a final attempt was made to land the ROV on the seafloor at a site 100 m east and therefore upstream of site 2 (Figures 1c and 1d, event h). At 20:43 UTM, the ROV landed on the seafloor in 388 m of water; the water was turbid, but the visibility was sufficient to see ripples on the seafloor. The ROV proceeded to locate and land within the thalweg (398 m) (Figures 1c and 1d, event i), where visibility was diminished due to a turbid flow that was observed to roll clumps of kelp over the bottom (Figures 1c and 1d, event j). Four minutes after landing in the thalweg, visibility increased sufficiently to see particles travelling as bed load across the seafloor. Visibility remained sufficient to see the seafloor for 7 min, after which, there was another pulse of more turbid water carrying clumps of kelp. At 21:04 UTM, deteriorating weather conditions on the surface required that the ROV be recovered. During the ascent (Figures 1c and 1d, event k), a sharp billowing interface with “clear water” was observed at 368 m water depth (see annotated video - clip #4), which was 30 m above the thalweg. On leaving the bottom for the final time, the water temperature had risen to 7.54°C, and salinity had reduced to 34.00 psu.

4.2. Turbidity and Velocity Profiles

4.2.1. Turbidity

Four BAC profiles, herein referred to as turbidity profiles, were reconstructed from the ROV transmissometer data: one background profile from site 1 prior to and during the earliest very dilute stages of the current (Figure 2a), one profile from site 2 where the current was first encountered (Figure 2b), and two profiles from site 4, the final location where the current was encountered (Figures 2c and 2d). The background turbidity profile is nearly vertical but increases slightly within 50 m of the seafloor (Figure 2a); this profile is typical of profiles from other submarine canyons during quiescent periods. The depth-averaged BAC of this “background” profile is 0.9 m^{-1} after removing the surface peak.

The final turbidity profile (Figure 2d) clearly demonstrates the two-layered anatomy of the flow. A 30 m thick lower layer with a depth-averaged turbidity of 1.9 m^{-1} is overlain by an 89 m thick dilute layer with a depth averaged turbidity of 1.0 m^{-1} that returns to a background turbidity of 0.9 m^{-1} at 278 m water depth. For reference, the maximum measured BAC of 5.17 m^{-1} in profile 2 represents a volume concentration in the range of 0.004–0.04%, assuming a grain size range of 63–150 μm . Thus, while we refer to the basal layer as

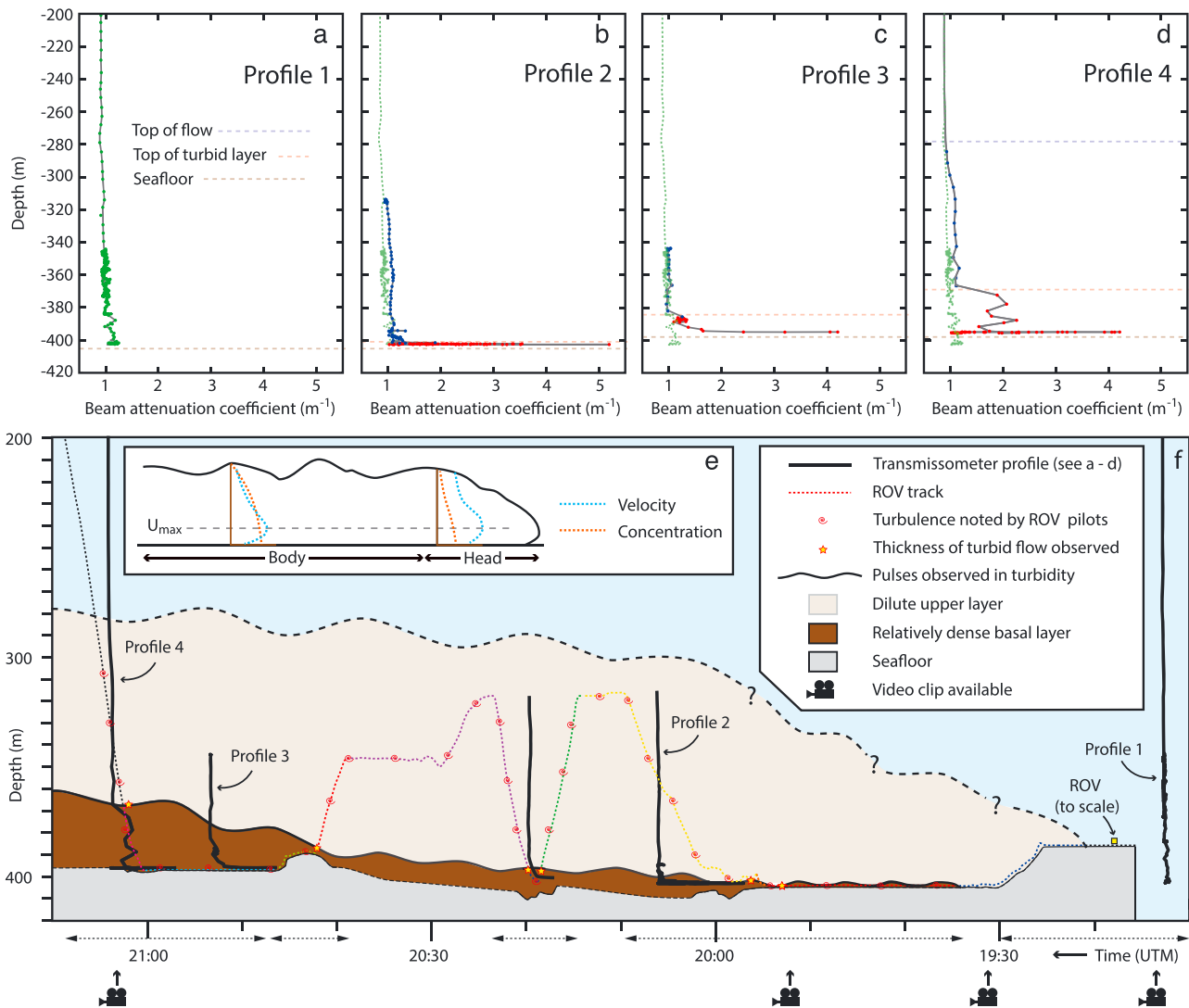


Figure 2. Profiles of depth versus beam attenuation coefficient (turbidity) (a) Profile 1 collected at site 1 prior to and during the earliest dilute stages of the turbidity current. The green dots show data used to calculate the background depth-averaged BAC. (b) Profile 2 at site 2. The blue and red dots show data used to calculate the depth-averaged BAC of dilute and turbid layers, respectively; the pale green hashed line shows the background profile from Figure 2a. (c) Profile 3 collected at site 4. (d) Profile 4 collected at site 4. (e) The idealized model of a turbidity current redrawn using data from *Baas et al.* [2005] and *Leeder* [2011]. (f) Model summarizing the key features of the turbidity current. The turbidity profiles are all to the same scale. The double headed arrows show the time range over which the profiles were collected. The coloration of the ROV track corresponds with the coloration of events a to k in Figure 1. Video clips are available at <https://www.youtube.com/watch?v=43Hp2ETgIXM>.

dense relative to the overlying layer, its absolute concentration is very dilute and of insufficient concentration for granular interactions to be important [*Amy et al.*, 2006].

The three turbidity profiles from sites 2 and 4 corroborate the visual observation that through time, the thickness of the turbid lower layer increased. The turbidity of the lower layer is 1.4 m^{-1} in profiles 2 and 3 (Figures 2b and 2c) and increases to 1.9 m^{-1} in profile 4 (Figure 2d). Given that BAC is linearly proportional to concentration, this represents a 36% increase in concentration. In contrast, the depth-averaged turbidity of the upper dilute layer fluctuates from 1.1 m^{-1} in profile 2 (Figure 2b) to 1.0 m^{-1} in profile 4a (Figure 2c) and then back to 1.1 m^{-1} in profile 4b (Figure 2d); this represents a 10% increase in concentration between the final two profiles. The BAC measurements demonstrate that the upper layer contained sediment in excess of background values; however, the video recordings are too insensitive to reliably detect such low concentrations of sediment.

4.2.2. Velocity

The velocity of the current was estimated from the sum of the velocity that the ROV was swept down canyon and the speed at which the ROV was flying against the current; the forward speed of the ROV at full thrust was ~1 m/s. Using this method, a velocity of ~1.7 m/s was measured 3.5 m altitude above the thalweg, while the ROV was being swept down canyon between sites 2 and 3. The thickness of the lower turbid layer at sites 2 and 3 varied between 0.5 m and 10 m; thus, the highest velocities occurred within the turbid lower layer. Velocities of ~1 m/s were also estimated for the upper dilute layer on the basis that the ROV struggled to fly up the canyon against the current.

5. Discussion

We interpret the event described above to have been a turbidity current on the basis that it was a sediment-laden, turbulent flow that moved downslope within the canyon. The turbidity current was up to 119 m thick, had an estimated maximum velocity of ~1.7 m/s, and concentration of <0.04 vol %; thus, it is comparable in scale to subannual turbidity currents measured in Monterey Canyon [Xu *et al.*, 2004, 2014; Talling *et al.*, 2013, Table 1] that dissipate within the canyon. It is likely that this flow left behind at most millimeter-scale deposits on the canyon floor; thus, it was a very small flow in comparison to the flows that laid down the decimeter- and meter-thick sand-rich turbidites that are common in the geological record.

5.1. Structure of the Turbidity Current

An important feature of this turbidity current is that it had two distinct layers: a thin and relatively dense basal layer overlain by a thick and dilute cloud. This is the first data showing distinct layers within a field-scale turbidity current and how those layers evolved through time. A simple model of the turbidity current based upon the above observations and measurements is shown in Figure 2f. This model assumes that sites 1 to 3 were sufficiently closely located to be considered as approximately the same location; this is justified because the maximum distance between the sites is <180 m, whereas the turbidity current is likely to have traveled for many kilometers.

The observations show that the turbidity current comprised two layers that we infer resulted from the interaction of two initial flow pulses. This inference is based on the structure of the flow front, which did not resemble the simple abrupt interface often depicted in textbook models. First, the front of the flow was not the fastest moving part of the flow; the faster moving basal layer lagged the flow front by 14 min. Experimental data suggest that the downslope advance of the head of a turbidity current is slower than the current velocities measured within their bodies [e.g., Kneller and Buckee, 2000]. However, the observed time lag of 14 min for a body estimated to move at 1.7 m/s requires the head of the flow to be ~1.4 km long, which is difficult to reconcile with classical conceptual models [e.g., Allen, 1985]. Second, the dilute layer, that included the flow front, was only observed to be turbulent when it occurred on top of the fast, turbulent, and relatively dense basal layer. This suggests a strong and rapidly acquired coupling between the two layers. Furthermore, the wedge shape of the lower relatively dense layer and the lack of a bulbous head are characteristics of a fast dense gravity current intruding into a slower less dense gravity current [Fernandez and Imberger, 2008].

Experiments suggest two possible fates for this turbidity current: either the two layers mix to form one layer or the lower relatively dense layer overtakes the front of the original flow with little or no mixing and becomes the new flow front [Gladstone *et al.*, 2004; Amy *et al.*, 2005; Fernandez and Imberger, 2008]. Which fate occurs is determined by the density difference between the two layers. Fernandez and Imberger [2008] define a density difference ratio (Δ^*): $\Delta^* = (\rho_1 - \rho_a) / (\rho_2 - \rho_a)$, where ρ_1 is the density of the initial dilute gravity current, ρ_2 is the density of the latter dense gravity current, and ρ_a is the density of ambient fluid: $\Delta^* > 0.5$ leads to mixing, whereas $\Delta^* < 0.4$ leads to the dense layer becoming the new flow front. The turbidity current in Mendocino Canyon had $\Delta^* \sim 0.26$ making it likely that the dense layer overtook the dilute layer and ultimately became the new flow front.

The lower dense layer was characterized by rhythmic oscillations in turbidity that were observed to correlate with changes in the thickness of the lower layer. These oscillations had a much longer length scale than the billows visually observed at the interface between the layers. Instabilities at the interface between moving fluids of different densities are widely recognized, including in some laboratory-scale gravity current

[Amy *et al.*, 2005] and turbidity current [Cartigny *et al.*, 2013] experiments. Such features have been attributed to Kelvin–Helmholtz instabilities or roll waves [Cartigny *et al.*, 2013].

5.2. Triggering

The turbidity current was not triggered by the ROV because the flow came down canyon from the east, whereas the ROV had been operating to the north (Figure 1c). No earthquakes shortly predated or correlated with the onset of the turbidity current [United States Geological Survey and California Geological Survey, 2014]. Given the weather conditions during the dive, the turbidity current may have been triggered by storm-wave loading of shelfal sediments during rough seas. Storm-wave loading does not necessarily represent an instantaneous turbidity current trigger, but instead, sediment may be periodically swept into the canyon head throughout the duration of the storm. We also observed relatively warm freshwater entering the canyon head prior to the onset of the turbidity current as has been observed on other margins [Ulses *et al.*, 2008]. Buoyant downwelling can result from water piling up at the coast during storms, thus creating a hydraulic head [Ulses *et al.*, 2008], or advection of a relatively buoyant oceanographic water mass over the canyon head. This water movement may have disturbed the bottom sediments and triggered the turbidity current. Ultimately, we are uncertain how the turbidity current was triggered.

5.3. Measuring Turbidity Currents in the Oceans

Cable breaks provide the only measurements of the largest turbidity currents that reach the deep ocean and deposit thick layers of sand on submarine fans [e.g., Piper *et al.*, 1999; Carter *et al.*, 2012]. Estimating flow velocities from cable breaks is based on the assumption that the cable is broken by the front of the turbidity current, and therefore, the timing of sequential cable breaks can be used to infer the frontal velocity of the turbidity current. However, if the flow front is complex, which is most likely in proximal locations, then the critical conditions to break the cable may be attained in the body rather than the head of the flow. Furthermore, there is no reason to assume that the critical conditions required to break a cable may not migrate spatially within the turbidity current as it evolves. While velocity estimates from cable breaks provide rare insights into the nature of turbidity currents, our data suggest that some caution should be attached to such estimates until the structure of turbidity currents is better understood.

This data set provides a new perspective on the character of turbidity currents in the ocean. The data pose challenges not simply for understanding the dynamics of turbidity currents but also for how we might measure similar flows in the future. These unorthodox measurements were collected by fortuitous chance, and it is sobering to consider what features of this flow would have been captured if there had been a conventional mooring in Mendocino Canyon Head on 3 August 2013. A typical mooring comprises an acoustic Doppler current profiler (ADCP) located ~70 m above the seafloor and a selection of other equipment such as CTD profilers, transmissometers, and sediment traps at fixed heights above the bed but rarely, if ever, within ~15 m of the seafloor due to the risk of damage to equipment [e.g., Xu *et al.*, 2014]. First, we would have no visual observations of the flow, which were important in interpreting the physical measurements. Second, we would have no measurements from within ~4 m of the seafloor, which we have demonstrated can contain relatively concentrated near-bed layers. Third, given battery constraints (e.g., hourly sampling intervals), the ~1.5 h of observations described here would be averaged into a few data points or profiles for each instrument. For example, Xu *et al.* [2013] had two ADCPs in Monterey Canyon spaced 14.5 km apart. One ADCP averaged 125 pings over a 40 min period; the other ADCP averaged 60 pings over a 1 min period at 10 min intervals. On a positive note, one or more moorings would have enabled measurement of profiles of velocity and backscatter that spanned the full duration of the turbidity current, albeit it is questionable how well the ADCP would have penetrated across the abrupt rheological interface and into the relatively dense lower layer. Moorings would also have enabled collection of samples detailing flow composition. There is a clear need for the development of innovative techniques to measure oceanographic turbidity currents, in particular with respect to penetrating into dense near-bed layers and improving the temporal resolution of measurements.

6. Conclusions

In this paper we present novel observations of a turbidity current, which was fortuitously encountered during an ROV dive in the head of Mendocino Canyon, California. We were able to observe the evolution of the turbidity current over 1.5 h.

The turbidity current had a total thickness of up to 119 m and comprised two distinct layers: the upper layer was thick (up to 89 m) and very dilute, whereas the lower layer was thin (0.5–30 m), fast (~1.7 m/s), and much denser than the upper layer, albeit its absolute density was still dilute (<0.04 vol %). The fast moving basal layer lagged the slower moving dilute flow front by 14 min. This observation combined with the wedge shape of the lower layer and the lack of bulbous head leads us to infer that the turbidity current originated as two separate pulses: an initial sluggish dilute flow that was intruded by a later faster higher density flow. The interface between the two layers was characterized by a wave-like instability. The lower layer was highly turbulent, whereas the upper layer was only observed to be turbulent once the lower dense layer had intruded it. This suggests an important coupling between the dynamics of the two layers.

We present a novel set of observations of an ocean turbidity current that provide unique insight into the complex structure of turbidity currents that should be considered in future experimental, numerical, and conceptual models. In addition, these observations highlight the need to develop suitable technologies to purposefully and systematically measure similar flows in the future.

Acknowledgments

The work was funded by the David and Lucile Packard Foundation. We thank the master, crew, and shipboard scientific party of the R/V *Western Flyer*. Special thanks are given to the MBARI ROV pilots for their great skill and willingness to fly the ROV in extremely demanding conditions. We thank Peter Talling and David Piper for their insightful reviews that improved the manuscript. The data used in this study are available upon request from Monterey Bay Aquarium Research Institute.

The Editor thanks Peter Talling and an anonymous reviewer for their assistance in evaluating this paper.

References

- Allen, J. R. L. (1985), Loose-boundary hydraulics and fluid mechanics: Selected advances since 1961, in *Sedimentology: Recent Developments and Applied Aspects*, edited by P. J. Brenchley and D. J. P. Swift, *Geol. Soc. London Spec. Publ.*, 18, 7–28.
- Amy, L. A., J. Peakall, and P. J. Talling (2005), Density- and viscosity-stratified gravity currents: Insight from laboratory experiments and implications for submarine flow deposits, *Sediment. Geol.*, 179, 5–29, doi:10.1016/j.sedgeo.2005.04.009.
- Amy, L. A., P. J. Talling, V. O. Edmonds, E. J. Sumner, and A. Lesueur (2006), An experimental investigation of sand-mud suspension settling behavior: Implications for bimodal mud contents of submarine flow deposits, *Sedimentology*, 53, 1411–1434, doi:10.1111/j.1365-3091.2006.00815.x.
- Baas, J. H., D. McCaffrey, P. D. W. Haughton, and C. Choux (2005), Coupling between suspended sediment distribution and turbulence structure in a laboratory turbidity current, *J. Geophys. Res.*, 110, C11015, doi:10.1029/2004JC002668.
- Carter, L., J. D. Milliman, P. J. Talling, R. Gavey, and R. B. Wynn (2012), Near-synchronous and delayed initiation of long run-out submarine sediment flows from a record-breaking river flood, offshore Taiwan, *Geophys. Res. Lett.*, 39, L12603, doi:10.1029/2012GL051172.
- Cartigny, M. J. B., J. T. Eggenhuisen, E. W. M. Hansen, and G. Postma (2013), Concentration-dependent flow stratification in experimental high-density turbidity currents and their relevance to turbidite facies models, *J. Sediment. Res.*, 83, 1046–1064, doi:10.2110/jsr.2013.71.
- Cooper, C., J. Wood, and O. Andrieux (2013), Turbidity current measurements in the Congo Canyon, in Proceedings of the Annual Offshore Technology Conference (OTC 23992).
- Fernandez, R. L., and J. Imberger (2008), Relative buoyancy dominates thermal-like flow interaction along an incline, *J. Hydraul. Eng.*, 134, 636–643, doi:10.1061/(ASCE)0733-9429(2008)134:5(636).
- Gladstone, C., L. J. Ritchie, R. S. J. Sparks, and A. W. Woods (2004), An experimental investigation of density-stratified inertial gravity currents, *Sedimentology*, 51, 767–789, doi:10.1111/j.1365-3091.2004.00650.
- Goldfinger, C., et al. (2007), Turbidite event history: Methods and implications for Holocene paleoseismicity of the Cascadia Subduction Zone, *U.S. Geol. Surv. Prof. Pap.* 1661-F, p. 170.
- Guillén, J., A. Palanques, P. Puig, X. Durieu de Madron, and F. Nyffeler (2000), Field calibration of optical sensors for measuring suspended sediment concentration in the western Mediterranean, *Sci. Mar.*, 64, 427–435.
- Hughes Clarke, J. E., C. R. Vidiera Marques, and D. Pratomo (2014), Imaging active mass-wasting and sediment flows on a fjord delta, Squamish, British Columbia. *Submarine Mass Movements and Their Consequences, Adv. Nat. Technol. Hazard. Res.*, 37, 249–260, doi:10.1007/978-3-319-00972-8.
- Kneller, B., and C. Buckee (2000), The structure and fluid mechanics of turbidity currents: A review of some recent studies and their geological implications, *Sedimentology*, 46, 62–94.
- Leeder, M. (2011), *Sedimentology and Sedimentary Basins: From Turbulence to Tectonics*, Wiley-Blackwell, Chichester, 767 pp.
- Piper, D. J. W., P. Cochonot, and M. L. Morrison (1999), The sequence of events around the epicenter of the 1929 Grand Banks earthquake: Initiation of debris flows and turbidity current inferred from sidescan sonar, *Sedimentology*, 46, 79–97.
- Puig, P., A. Palanques, and J. Martín (2014), Contemporary sediment-transport processes in submarine canyons, *Ann. Rev. Mar. Sci.*, 6, 53–77, doi:10.1146/annurev-marine-010213-135037.
- RDI Instruments (2014), Glossary, accessed from RDI Instruments website: Accessed 1 September 2014. [Available at <http://www.rdinstruments.com/glossary.aspx>]
- Sea-Bird Electronics (2011), Application Note No. 91: Calculating Calibration Coefficients for wet c-star Transmissometer (voltage or RS-232 output sensor) 3p.
- Talling, P. J., C. K. Paull, and D. J. W. Piper (2013), How are subaqueous sediment density flows triggered, what is their internal structure and how does it evolve? Direct observations from monitoring of active flows, *Earth Sci. Rev.*, 125, 244–287, doi:10.1016/j.earscirev.2013.07.005.
- Ulses, C., C. Rstournel, J. Bonnin, X. Durrieu de Madron, and P. Marsaleix (2008), Impact of storms and dense water cascading on shelf-slope exchanges in the Gulf of Lion (NW Mediterranean), *J. Geophys. Res.*, 113, C02010, doi:10.1029/2006JC003795.
- United States Geological Survey and California Geological Survey (2014), Quaternary fault and fold database for the United States. [Accessed May 6 2014, from USGS web site: <http://earthquake.usgs.gov/hazards/qfaults/>]
- Xu, J. (2010), Normalized velocity profiles of field-measured turbidity currents, *Geology*, 38, 563–566, doi:10.1130/G30582.1.
- Xu, J. (2011), Measuring currents in submarine canyons: Technological and scientific progress in the past 30 years, *Geosphere*, 7, 868–876, doi:10.1130/GES00640.1.
- Xu, J. P., M. A. Noble, and L. K. Rosenfeld (2004), In-situ measurements of velocity structure within turbidity currents, *Geophys. Res. Lett.*, 31, L09311, doi:10.1029/2004GL019718.
- Xu, J. P., J. P. Barry, and C. K. Paull (2013), Small-scale turbidity currents in a big submarine canyon, *Geology*, 41, 143–146, doi:10.1130/G33727.1.
- Xu, J. P., O. E. Sequeiros, and M. Noble (2014), Sediment concentrations, flow conditions, and downstream evolution of two turbidity currents, Monterey Canyon, USA, *Deep Sea Res., Part 1*, 89, 11–34, doi:10.1016/j.dsr.2014.04.001.